

# Three Years of ChaMPlane Northern Field WIYN Spectroscopy

A. B. Rogel, P. M. Lugger, H. N. Cohn

*Department of Astronomy, Swain Hall West 319, Indiana University, 727 E. 3rd. St.,  
Bloomington, IN 47405*

abrogel@astro.indiana.edu

S. D. Slavin

*Department of Chemistry and Physics, Purdue University Calumet, 2200 169th St.,  
Hammond, IN 46323-2094*

J. E. Grindlay, P. Zhao, J. Hong

*Harvard-Smithsonian Center for Astrophysics, 60 Garden St., Cambridge, MA 02138*

## ABSTRACT

We present initial results of WIYN spectroscopic observations of selected objects detected in the *Chandra* Multiwavelength Plane (ChaMPlane) Survey in fields towards the Galactic anti-center. ChaMPlane is designed to identify low luminosity X-ray sources, both accretion-powered and stellar coronal, in the Galaxy. It also includes a wider-fields optical imaging Survey conducted with the NOAO Mosaic cameras to identify optical counterparts as well as H $\alpha$ -selected objects in the  $\sim 5\times$  larger field. We report spectra for 1048 objects in galactic anti-center (i.e. northern) fields, resulting in 609 type determinations. These include 5 new cataclysmic variables, 4 Be stars, 14 lithium-absorption stars, 180 stellar coronal sources (primarily dMe stars), and 29 new quasars. Bright optical counterparts of *Chandra* sources in this sample are most frequently dMe stars whereas a majority of the faintest ( $R \sim 21$ ) spectroscopically classified *Chandra* source counterparts are quasars. The bulk of H $\alpha$ -selected sources appears to be roughly evenly divided between dMe stars and M stars at all magnitudes.

*Subject headings:* binaries: close—cataclysmic variables—Galaxy: stellar content—quasars: general—stars: emission line, Be—surveys

## 1. Introduction

The ChaMPlane Survey (Grindlay et al. 2003, 2005) is designed to detect and optically identify low luminosity X-ray point sources in the Galactic plane. ChaMPlane is conducted in two phases: the ChaMPlane X-ray survey of serendipitous sources in *Chandra* X-ray Observatory archival deep ( $>20$  ksec) Galactic plane ( $|b| < 12^\circ$ ) fields, and the ChaMPlane Optical Survey of deep  $V$ ,  $R$ ,  $I$ , and  $H\alpha$  images of fields taken at CTIO or KPNO with the 4m telescope Mosaic ( $36' \times 36'$ ) cameras centered on the *Chandra* fields. Detailed descriptions of the X-ray detections and database are given by Hong et al. (2005), and the optical imaging, astrometry, and photometry with Mosaic are described by Zhao et al. (2005).

The ChaMPlane X-ray Survey takes advantage of the unparalleled angular resolution and  $\sim 1''$  absolute astrometry of the *Chandra* X-ray Observatory to match the serendipitous X-ray sources in the field with faint ( $R < 24$ ) optical counterparts. In all but the most crowded fields, nearly all matches are unambiguous. The point-source sensitivity for a typical 30 ksec ChaMPlane exposure allows detection of sources with  $L_X \gtrsim 10^{31}$  ergs $^{-1}$  at 8 kpc, which enables detection of cataclysmic variables (CVs), one of the prime ChaMPlane objectives, throughout a significant fraction of the Galaxy. Grindlay et al. (2003) and Zhao et al. (2003) have reported early results from the ChaMPlane X-ray Survey and followup optical photometry.

The ChaMPlane Optical Survey provides optical photometric followup of the *Chandra* serendipitous sources, providing  $H\alpha - R$ ,  $R - I$ , and  $V - I$  colors for the X-ray sources. By definition, stars without  $H\alpha$  emission should have an average  $H\alpha - R$  color index of  $\sim 0.0$ , while CVs and other accretion-powered systems frequently have significant  $H\alpha$  excesses, which register as negative  $H\alpha - R$  colors. This enables us to select objects that are  $H\alpha$  and/or X-ray bright for followup spectroscopy and classification.

The ChaMPlane Optical Survey will include all *Chandra* fields (observed with either the ACIS-I or ACIS-S cameras, with  $16' \times 16'$  and  $8' \times 8'$  fields, respectively) in the ChaMPlane X-ray Survey. The highest priority for the spectroscopic followup is to obtain spectra on each X-ray source optical counterpart with possible  $H\alpha$ -emission; the second priority is to obtain spectra on *all* *Chandra* source optical counterpart candidates, regardless of  $H\alpha$ -emission status. Since the Mosaic camera has a field of view about 4.5 times larger in area than the ACIS-I, the Optical Survey will also detect many  $H\alpha$ -emission sources with unknown X-ray emission status. Thus, as a third priority, spectroscopy is also performed on these objects, since Hydra can simultaneously observe 60–70 objects, which (for the anti-center fields at least) enables us to observe all  $H\alpha$ -emission candidates in the ChaMPlane Optical Survey field in just one or two Hydra setups.

The ChaMPlane Optical imaging program is described in detail by Zhao et al. (2005). Normally, three (for  $V$  and  $I$ ) or five (for  $R$  and  $H\alpha$ ) dithered exposures are taken and combined to remove cosmic rays and other image contamination. Total exposure times are set to enable 5–7% precision photometry to 24th magnitude in all bands. Short exposures in each band are also taken to give unsaturated data for the brighter objects. Mosaic data reduction and analysis is done using standard IRAF<sup>1</sup> *mscred* tasks, and photometry with DAOPHOT.

In this paper, we report initial results for followup spectroscopy carried out with the WIYN<sup>2</sup> Hydra multi-object spectrometer. This paper is organized as follows: §2 describes the observing and analysis procedures, with spectroscopic results presented in §3. We summarize our results in §4. In Rogel et al. (2005), we discuss some of the implications of our anti-center field results for the space density of CVs, using a Monte-Carlo model of the CV distribution within the Galaxy. Laycock et al. (2005) discuss the combined X-ray and optical (both photometric and spectroscopic) constraints on the total *Chandra* source populations in the anti-center fields, as well as X-ray properties of individual classes of objects.

## 2. Data Acquisition and Reduction

### 2.1. Field Selection

Brief summaries of the 13 fields observed with WIYN/Hydra to date are given in Table 1. Of these 13 fields, 11 are in the general Galactic anti-center direction (quadrants 2 and 3, i.e. galactic longitude  $90^\circ \leq l \leq 270^\circ$ ), as seen in Figure 1. Eight of the fields lie within  $45^\circ$  of the Galactic anticenter. The two fields in the first quadrant (Sgr1900+14 and MWC297) are included since their northern declination allowed them to be observed from WIYN. These two first quadrant fields still sample pure disk volumes, as the Galactic bulge extends only to about 3 kpc (Binney & Merrifield 1998), which corresponds to about  $l = 22^\circ$ . An extensive program of photometry and spectroscopy on Galactic bulge fields is also being conducted by ChaMPlane and will be reported in subsequent papers.

---

<sup>1</sup>IRAF is distributed by the National Optical Astronomy Observatories, which are operated by the Association of Universities for Research in Astronomy, Inc., under cooperative agreement with the National Science Foundation.

<sup>2</sup>The WIYN Observatory is a joint facility of the University of Wisconsin, Indiana University, Yale University, and the National Optical Astronomy Observatories.

## 2.2. Spectroscopic Target Selection

Each *Chandra* field was observed with the CTIO or KPNO 4m in the  $V$ ,  $R$ ,  $I$ , and  $H\alpha$  bands with the Mosaic ( $36' \times 36'$ ) camera. Target lists were created for both X-ray and  $H\alpha$  objects. The X-ray target list is composed of objects detected in the *Chandra* observation which have optical counterparts in the combined  $R$ -band image, which is the deepest of the four bands. An X-ray source is considered to match an optical source if the position offset is less than a variable offset allowance, derived from the optical astrometry error ( $< 1''$ ), X-ray–optical boresite error ( $< 1''$ ), and the X-ray astrometry ( $\sim 0.3''$  for the best case of a bright source near the instrument axis, and up to  $4''$  for faint objects far from the instrument axis). The maximum offset allowance is  $4''$ , but sources near the ACIS axis have offset allowances as small as  $1''$ . Roughly 50% of *Chandra* sources in these 13 anti-center fields have optical counterparts with  $R < 23$  (Zhao et al. 2003). Details of the astrometry and optical vs. X-ray matches are given by Zhao et al. (2005) and Laycock et al. (2005).

The  $H\alpha$ -definite target list is composed of objects selected by  $H\alpha-R$  color, with  $H\alpha-R \leq -0.3$  defined as the minimum threshold for objects of definite interest. Given the KPNO MOSAIC filter bandpass data for the  $H\alpha$  and  $R$  filters, our threshold corresponds to  $EW(H\alpha) \sim 28 \text{ \AA}$ , using a flat continuum spectrum with  $H\alpha$  emission added at  $6563 \text{ \AA}$ . This criterion allows us to reject most normal stars, while retaining potential strong  $H\alpha$ -emission CV candidates. However, many normal M and dMe stars are selected by this criterion, as a result of the strong TiO absorption bands on either side of  $\sim 6500 \text{ \AA}$ . A separate  $H\alpha$  target list (the  $H\alpha$ -marginal, or  $H\alpha M$ , list) is composed of objects with  $H\alpha-R$  color between  $-0.2$  and  $-0.3$ , or  $EW(H\alpha)$  between  $17 \text{ \AA}$  and  $28 \text{ \AA}$ . These targets are of lower interest, since the object is more likely to be a normal star due to the spread in the  $H\alpha-R$  distribution.

*Chandra* sources which are also  $H\alpha$  targets receive highest priority for the assignment of Hydra fibers, as these are the most promising X-ray binary or CV candidates. All remaining *Chandra* sources with optical counterparts with  $R < 22$ , and thus accessible to WIYN/Hydra, are given second priority for fiber assignment. Third in priority are  $H\alpha$  sources with no *Chandra* detection, usually due to their being outside the *Chandra* field of view, which is  $5\times$  smaller in area than the Mosaic image field. However, some of these objects are within the *Chandra* field but are not detected owing to X-ray flux emission below  $L_X = 10^{31} \text{ ergs}^{-1}$ . Lowest priority is assigned to the  $H\alpha$ -marginal targets. Before final assignment, the Mosaic image positions for each selected Hydra target are manually verified to check for source confusion, cosmic ray contamination, and other problems.

ChaMPlane source naming follows the following convention (cf. Grindlay et al. 2005): all X-ray sources are designated with a CXOPS (Chandra X-ray Observatory Plane Survey) prefix, followed by J2000 X-ray coordinates JHHMMSS.S+DDMMSS. All optical sources

are designated with a ChOPS (Chandra Optical Plane Survey) prefix, followed by optical coordinates JHHMMSS.SS+DDMMSS.S. For an X-ray source with an optical counterpart, the CXOPS and ChOPS coordinates can differ by up to the offset allowance discussed above owing to the different sources for the coordinates. As all X-ray sources selected for follow-up spectroscopy have optical counterparts, they will have both CXOPS and ChOPS designations. In this paper, only the CXOPS designation is used for objects with *Chandra* detections. Objects referred to by a ChOPS designation in this paper include H $\alpha$ -emission objects selected for spectroscopy but for which there is either a *Chandra* non-detection or no *Chandra* measurement at all. Both the CXOPS and ChOPS catalogs cross-reference each other and be released in future papers.

### 2.3. Spectroscopic Observations

All the spectra presented here were taken with the Hydra fiber-fed multi-object spectrograph on the 3.5m WIYN telescope. Hydra has two fiber bundles, with different-sized fibers, optimized to work at different wavelength ranges. We chose to use the red bundle, which has smaller fibers (2" diameter versus 3" for the blue fibers), to reduce the impact of skylight on the spectra. This, along with the bench spectrograph's CCD sensitivity profile, results in severely diminished blue sensitivity. As we are primarily interested in H $\alpha$ , at 6563 Å, and nearby helium lines, this is an acceptable compromise.

Field setup is done with the *whydra* program. ChaMPlane objects are assigned to fibers with the priorities given above. Each sublist is sorted by R-band magnitude to give preference to bright objects. About 15-25 sky positions are used, as well as a minimum of 6 FOPS (guide stars), leaving 65-75 object fibers available. The *whydra* output is then tuned by hand using the *hydrasim* package to optimize fiber usage, resulting in about 65 objects per field setup.

We use the 600@10.1 "Zepf" blue-blazed grating for Hydra, which results in a resolution of 1"4/pixel. We target a wavelength range of 4000–6800 Å, which gives us good coverage of the first few Balmer lines and the helium lines at 4686 Å, 5875 Å, and 6678 Å, while avoiding the extremely bright comparison-lamp line at 6965 Å. This enables us to take a single comparison exposure with good S/N over the entire wavelength range. The typical observing procedure is to take multiple sets of two long (2400 – 3600 sec) exposures, with each set bracketed by 200 sec CuAr comparison lamp exposures. This minimizes the time lost to calibration, while still allowing for correction of wavelength drift over the night. To minimize the effect of cosmic rays, at least 5 exposures are taken, with the available time split to allow for this. This results in a total of 3.5–7 hours of exposure per setup. Some

fields have enough objects that multiple setups are necessary, which allows for longer total exposure time on fainter objects and objects of particular interest. Depending on the season, 1–2 setups per night are observed.

## 2.4. Reduction Procedure

The basic data reduction process consists of preliminary image processing using the IRAF *ccdproc* package (for bias subtraction), followed by spectral reduction using the IRAF *dohydra* package. Standard procedures were followed, with dome flats used both for aperture reference and flat fields. Sky editing was used to remove problematic sky fibers. Bracketing comparison spectra were always used in the reduction process. Combination of the resulting spectra was done with a median filter to eliminate cosmic rays.

For the B2224, J2227, G116, MWC297, and PSRJ0538 fields, the  $H\alpha$  image showed substantial variations in the background signal, resulting from Galactic diffuse emission in  $H\alpha$ , N II, and S II. For the case of the fields with this diffuse emission, the basic reduction process results in the subtraction of an *average* (sky + Galactic diffuse) emission level from all of the spectra. As the Galactic diffuse emission level varied across the field, this process generally results in over- or under-subtraction of the diffuse emission in each individual spectrum. As we are specifically interested in the  $H\alpha$  emission levels of the targets, this can be a serious problem, as became clear from the first observation of the B2224 and J2227 fields in August 2002. We therefore remove the Galactic diffuse emission signal by taking spectra of sky positions offset by a few arcseconds from the target object. Offset positions were selected by careful inspection of the deep  $R$  image, in order to maximize faint object detection to ensure clear sky locations. In addition, the deep  $H\alpha$  frame was used to pick a location for the offset fiber that had the same (or as close as possible) Galactic diffuse emission as the object location. This proved especially important in the few cases where there was a supernova remnant in the Mosaic image. Fibers originally targeted at sky positions were not moved and thus provide a measure of any change in the sky brightness between the “on” and “off” exposures.

The following outlines the general method used to recover the object spectrum from the observations, with actual observations indicated with parentheses.

- “GDE” = Galactic Diffuse Emission
- “Sky” = *average*(GDE + local sky) for sky-fiber positions
- “On” = (Object + GDE + local sky) – Sky

$$\begin{aligned} \text{“Off”} &= (\text{GDE} + \text{local sky}) - \text{Sky} \\ \text{“Object”} &= \text{On} - \text{Off} \end{aligned}$$

Typically, about 1 hour of observing time is devoted to the offset positions, split into 5 separate observations to enable good cosmic ray removal. As a consistency test, the residual line emission in the sky fibers (which are not moved between the “on” and “off” setups) is checked to ensure that it falls within the general expected noise level. This method has been applied with good success since the 2002 Dec 5 run.

In cases where we experienced poor weather during a run in which this method was used, we simply looked at the line ratios in the diffuse Galactic emission, versus the same line ratios in the object spectrum. In several cases, the  $\text{H}\alpha$  vs.  $[\text{N II}]\lambda 6548.1 \text{ \AA}$  or  $[\text{S II}]\lambda 6716.4 \text{ \AA}$  and  $\lambda 6730.8 \text{ \AA}$  ratios have been substantially higher or lower in the object than in the offset spectrum, indicating clear  $\text{H}\alpha$  emission or absorption in the object. Subsequent application of the offset method during a later run has supported the positive emission classifications of this ratio method.

Classification of objects is done by visual inspection of reduced spectra. For CVs, we expect to see strong Balmer emission, possibly with split profiles, He I emission, and possibly He II emission. Other objects, such as T Tauri stars and M dwarf flare stars, can have both Balmer and He I emission, but usually with (much) narrower lines. Thus, additional criteria are needed to distinguish between these and likely CV candidates. The presence of lithium absorption is used to distinguish T Tauri (or other young star) candidates, and the FWHM of the  $\text{H}\alpha$  line is used to determine flare-star candidacy. Our narrowest line CV candidate, which shows a split  $\text{H}\alpha$  profile, has a FWHM of  $10 \text{ \AA}$ . The one flare-star candidate (with both Balmer and He I emission) has an  $\text{H}\alpha$  FWHM of  $4.5 \text{ \AA}$ . Comparison with published spectra was used for spectral classification of stars. Quasar redshifts were determined by comparing emission line wavelengths to those given by Vanden Berk et al. (2001).

### 3. Spectral Results

#### 3.1. Overview

To date, we have observed 13 fields over 17 nights, with multiple setups on some fields. A summary of the observing runs is given in Table 2. Table 3 lists the total, observed, and classified number of objects for each target list, summed across all fields. Five new CV candidates were detected within the  $\text{H}\alpha$ -definite list. Of the 14 objects designated as ‘duplicates’, seven appear on both the X-ray and  $\text{H}\alpha$ -definite list, and seven appear on both

the X-ray and  $H\alpha$ -marginal list. The ‘other’ list is a set of objects that were observed early in the spectroscopic program, but that were subsequently dropped from the target lists as a result of refinements of the targeting criteria. In general, about 50% of targets can be classified, with classification failure primarily due to the WIYN magnitude limit. The  $H\alpha$ -marginal list has a much higher classification rate, owing to selection of the brighter marginal objects to fill out a field. Figure 2 shows the classification rate as a function of target magnitude, demonstrating that we have near-complete classification of objects brighter than  $R = 20$ . We can generally classify about half of the objects as faint as  $R = 21.5$ , and in some cases can classify objects as faint as magnitude 23.5. These latter objects are typically those with very strong emission characteristics, such as narrow-line quasars.

As a check of our  $H\alpha - R$  cutoffs for  $H\alpha$ -definite and  $H\alpha$ -marginal targets, we looked at object classifications binned by  $H\alpha - R$  color (Figure 3). All five CV candidates, the two known LMXBs, and three of four Be stars are found to have  $H\alpha - R$  color  $\leq -0.3$ , and all the CV/LMXBs but A0620-00 have  $H\alpha - R$  color  $\leq -0.5$ . Only one Be star is found with an  $H\alpha - R$  color between  $-0.3$  and  $-0.2$ . Nearly all M and K stars of all types have measured  $H\alpha - R$  color  $\geq -0.4$ , with most being  $\geq -0.3$ . Thus, with the placement of the  $H\alpha - R$  cutoffs, we achieve our goal of limiting the selection of typical stars while not excluding our objects of prime interest. As expected, our quasars usually have a near-zero apparent  $H\alpha - R$  color, as only certain specific values of redshift will cause a typical quasar or AGN emission line to be located within the  $H\alpha$  bandpass. There appears to be no correlation between the photometrically-determined  $H\alpha - R$  color and the spectroscopically-determined emission status for M/K stars. As the  $H\alpha$  emission of dMe stars is known to vary by a factor of 2 on a timescale of a day (Reid & Hawley 2000), and these objects are also flaring objects, this lack of a correlation is not unexpected. Variability could also explain why the Be star in the 3C 129 field was on the  $H\alpha$ -marginal target list. Spectra for our newly-discovered CV candidates and a representative sample of the other interesting object classes are given as Figures 4-9. As we are primarily interested in simply classifying these objects, all spectra shown are NOT flux-calibrated.

### 3.2. CVs

Figure 4 shows the five CV candidates (all outside the *Chandra* field of view, but in the Mosaic field) discovered to date using WIYN/Hydra, while Table 4 lists the reference numbers and basic parameters for all five CV candidates and two previously-known LMXBs observed so far. Figure 5 shows the  $H\alpha$  and He I  $\lambda 6678$  Å regions for all new CV candidates.

CV #3 exhibits broad, split-profile  $H\alpha$  and He I emission lines, making it the clearest



candidate for CV status. The  $H\alpha$  line split gives a  $v \sin i$  rotation of 480 km/s.

CV #2 and CV #4 both have broad Balmer and He I lines, without showing the split profile. However, Galactic diffuse emission is present in CV #2, causing the narrow spike in the center of the  $H\alpha$  emission line and potentially filling a split line, and the CV #4 spectrum is noisy, so a split profile could be masked in both cases. CV #2 also exhibits the higher-excitation line He II  $\lambda 4686 \text{ \AA}$ .

CV #5 is similar to CV #2, with very weak evidence for the He II  $\lambda 4686 \text{ \AA}$  line. The spectrum is quite noisy, as we only have one hour of data. Acquisition of more data on this object is planned for Fall 2004.

CV #1 only shows a narrow  $H\alpha$ -emission feature, but it has a resolved, split peak characteristic of an accretion disk, and the signal is low enough that the other lines might be buried in the noise. The narrow  $H\alpha$  line split gives a  $v \sin i$  rotation of just 130 km/s, which, if one assumes rotational properties similar to CV #3, gives a maximum inclination of just  $15^\circ$ . Comparing the weak, mid-M star continuum profile of this source to other M stars in the same field gives an estimated magnitude for the secondary of  $R = 21.7 \pm 0.2$ . Using the absolute magnitudes for M dwarfs given by The, Steenman, & Alcaïno (1984), we get a distance of  $1200 \pm 600 \text{ pc}$ , assuming a secondary spectral type of between M2 and M6 and a constant extinction in  $R$  of 0.97 magnitudes per kpc (Binney & Merrifield 1998).

### 3.3. Be stars

Table 5 gives the basic parameters of the four Be star candidates classified with our WIYN spectra. While two of these objects were located within the ACIS field of view, no X-ray detections were made of these targets, thus eliminating them as HMXB candidates. All are spectrally similar to the ‘classical’ Be star of Porter & Rivinius (2003), which is a rapidly-rotating massive (late O to early A) star which creates an equatorial disk in some as yet poorly-understood manner. Figure 6 shows an example Be star candidate spectra. Of note in the spectrum is the apparently split  $H\beta$  line (Figure 6, panel a), which is the result of partial filling of the photospheric absorption line by the envelope emission. Given the relative strengths of the three lines ( $H\gamma$ , He I  $\lambda 4471 \text{ \AA}$ , and Mg II  $\lambda 4481 \text{ \AA}$ ), as seen in inset panel (b) of Figure 6, it appears that this star is likely to be spectral type B5 (Steele, Negueruela, & Clark 1999). Assuming the constant extinction of 0.97 mag/kpc in  $R$  as above, and using estimates for absolute magnitudes (ESA 1997) and color (Winkler et al. 1997) from the literature, we derive a distance of  $2300 \pm 300 \text{ pc}$ . The other three Be stars are fainter, and therefore have computed distances of 4–6 kpc. These distances are actually

underestimates, since the Be stars are located in fields in the second quadrant, i.e. outside the solar circle, and thus the extinction is most likely lower than assumed. The detection of Be stars at only the bright end of our available magnitude range, in our mostly quadrant two and three fields, is a result of a lack of star formation regions in the far reaches of the Galactic disk.

### 3.4. Lithium absorption stars

A total of 15 objects show clear lithium absorption with equivalent widths of 0.2–0.6 Å. Table 6 lists their parameters. Other than the lithium-abundant LXMB A0620-00 (González Hernández, et al. 2004), these stars are all simply classified as Lithium stars. Some show additional spectral features (as in Figure 7) allowing for further classification (most likely as T Tauri stars), while others show normal stellar continuum profiles, potentially being either very young main sequence stars, carbon stars (e.g. Hatzidimitriou et al. 2003), or late-type giants (e.g. Drake, et al. 2002). Of the 10 Lithium stars located within the *Chandra* field of view, 8 were detected as X-ray sources. Further discussion of the X-ray properties of these objects will be included in Laycock et al. (2005).

Figure 7 shows an example of a spectrum showing strong clear lithium absorption, along with many strong emission features. Figure 7, inset panel (a) shows the spectrum from 6400–6800 Å, which shows several iron emission lines as well as the lithium absorption. It is likely that this object is a T Tauri star, based on the similarities exhibited between it and the spectrum of DR Tau (Smith et al. 1999).

### 3.5. Coronal emission stars

A total of 433 M and K stars have been classified to date, with 180 being classified as clear emission objects. At present, we classify an object as an H $\alpha$ -emission object if it has clearly detectable H $\alpha$  emission when the spectrum is examined by eye. A further 40 objects have possible H $\alpha$  emission, but contamination by diffuse Galactic emission precludes definitive classification. A pair of sample spectra is given in Figure 8. Both stars are of similar spectral type (about M3, based on Fig. 2.2 in Reid & Hawley 2000), but H $\alpha$  emission of equivalent width  $\sim 5$  Å is present in ChOPS J062246.58-000949.8. H $\beta$  and H $\gamma$  are also present, with similar equivalent widths. One object of interest is ChOPS J182841.47-040535.6, which has an early-M type profile with both Balmer and He I  $\lambda 6678$  Å and  $\lambda 5875$  Å emission lines. The H $\alpha$  line is extremely strong, with equivalent width  $\sim 90$  Å. Based on

similarities to flare star emission lines reported by Gizis, Reid, & Hawley (2002), this object is most likely a flaring M star. As it fell outside the *Chandra* field of view, we have no X-ray data for this object. A full catalog of these objects, with equivalent width determinations and dwarf/giant differentiation, will be forthcoming in later publications of the project.

### 3.6. Quasars & AGN

A final serendipitous result of the ChaMPlane project is the discovery of 29 quasars or lower luminosity active galactic nuclei (AGN), 24 of which were detected as X-ray emission objects. Specific data on each quasar detected during the project to date are given in Table 7, with all CXOPS quasars being X-ray detections. While not ideal for quasar detection owing to obscuration in the Galactic plane, the ChaMPlane project has nevertheless been quite successful in detecting these objects. Quasars with redshifts ranging from 0.02 to 4.25 have been observed, with representative spectra shown in Figure 9. The classification of a spectrum as a quasar is conservatively based on being able to find a minimum of two emission features corresponding to lines in the composite quasar spectrum of Vanden Berk et al. (2001). Most quasars are detected as X-ray sources, with five being detected as apparent  $H\alpha$  sources. Two of these ‘ $H\alpha$ ’ objects are narrow-line AGN, possibly Seyfert IIs (like Figure 9 panel (h), by comparison with Seyfert II spectra in Moran, Filippenko, & Ryan 2002), and three are high-redshift broad-line objects. Of these three, two lie within the *Chandra* field of view but were not detected as X-ray sources, thus they must be weak X-ray emitters. The narrow-line AGNs and the other broad-line AGN lie outside the *Chandra* field, so we have no X-ray data on these three sources. In all cases, the ‘ $H\alpha$ ’ detection is actually another line redshifted into the narrow wavelength range of the  $H\alpha$  filter. Our WIYN/Hydra spectroscopic program is limited in quasar detection to those with redshifts less than about 4.6, owing to the shift of  $Ly\alpha$  past our red spectral limit of 6800 Å at higher redshift. Thus, quasars at higher redshifts would have a very low, nearly featureless continuum present in our spectra, and would not be able to be classified. Fainter quasars at a redshift around 1.0 will also not be detected by our spectroscopy, as there is only one major emission feature (Mg II  $\lambda 2798$  Å) available. Without secondary lines, such as in Figure 9 panel (f), a positive quasar classification with redshift determination cannot be made.

Examination of our quasar data reveals that 16 of 29 quasars are located in a single field. This field, J0422+32, has the lowest average  $E(B-V)$  of any field in the survey. Additionally, examination of the spectra shows that this interstellar gas is concentrated in a portion of the field, leaving the rest of the field with extremely low interstellar extinction as compared to other fields. This is also seen in the extinction map of the region based on data from Schlegel,

et al. (1998). The Chandra Multiwavelength Project (ChaMP), which is an extragalactic serendipitous *Chandra* source AGN survey, reports an average of 10 AGN per *Chandra* field, with 12 fields surveyed (Silverman et al. 2003). For our J0422 field, 11 of the 16 quasars are detected by X-ray emission, and two more lie within the *Chandra* field of view. Therefore, the J0422 field is similar in quasar detection rates to non-Galactic Plane fields, supporting the inference of extremely low interstellar extinction in most of this field. A detailed investigation of the ChaMPlane AGN, comparing their X-ray and optical properties, will be published separately.

#### 4. Discussion and Conclusions

On examination of the overall data set, some trends are evident in the object classifications. All of our five CV candidates are located in the 80% of each field imaged only with the Mosaic camera, and thus only show up on the  $H\alpha$  lists. The two known LMXBs showed up, as expected, on both the  $H\alpha$  and X-ray target lists. The Be stars discovered so far are all at the very bright end of our target objects, owing to the concentration of star forming activity within the solar circle.

The five new CVs and two known LMXBs are distributed across the surveyed magnitude range. Most quasars are optically faint X-ray objects, as would be expected from the strong increase of quasar counts with redshift. Coronal emission stars make up the bulk of the brighter X-ray targets, with some nearby normal (non-emission) stars at the very brightest end of our magnitude range. Both  $H\alpha$  lists contain primarily late-type stars, with about 45 – 50% (in the  $H\alpha$ -definite list, with  $H\alpha - R < -0.3$ ) and about 30 – 45% (in the  $H\alpha$ -marginal list, with  $-0.3 < H\alpha - R < -0.2$ ) appearing as coronal emission objects regardless of magnitude. The predominance of late-type stars in our  $H\alpha$ -selected sample is not surprising, given the locations of the strong TiO absorption bands in the continuum of the M-star spectrum at about  $H\alpha$  causing them to have an  $H\alpha - R$  color closer to our threshold value than earlier-type stars.

In summary, during the first three years of followup spectroscopy of northern fields for the ChaMPlane project, we have found five new CV candidates, four new Be star candidates, 14 lithium-absorption stars, 29 new quasars, and many new coronal emission objects. While at this time the total number of CVs detected is small, we have shown that our program of initial Mosaic photometry and followup WIYN-Hydra spectroscopy detects CVs in a systematic fashion. The larger samples expected from the full ChaMPlane survey will allow a volume-limited sample determination of the CV space density. Our serendipitous discoveries of Li stars, AGN, and substantial numbers of coronal emission stars will all lend themselves

to extensive further investigation.

This research was supported in part by NSF grant AST-0098683, NASA/Chandra grants AR2-3002B, AR3-4002B, and AR4-5003B. ABR gratefully acknowledges a fellowship from the Indiana Space Grant Consortium.

## REFERENCES

- Binney, J. & Merrifield, M. 1998, *Galactic Astronomy* (Princeton: Princeton University Press)
- Callanan, P. J., Garcia, M. R., McClintock, J. E., Zhao, P., Remillard, R. A., & Haberl, F. 1996, *ApJ*, 461, 351
- Drake, N. A., de la Reza, R., da Silva, L., Lambert, D. L. 2002, *AJ*, 123, 2703, astro-ph/2020158
- ESA 1997, *The Hipparcos and Tycho Catalogues*, ESA SP-1200
- Gizis, J. E., Reid, I. N., & Hawley, S. L. 2002, *AJ*, 123, 3356, astro-ph/0203499
- González Hernández, J. I., Rebolo, R., Israelian, G., Casares, J., Maeder, A., & Meynet, G. 2004, *ApJ*, 609, 988, astro-ph/0403402
- Grindlay, J. E., et al. 2003, *Astron. Nachr.*, 324, 57, astro-ph/0211527
- Grindlay, J. E., et al. 2005, in preparation
- Haswell, C. A. Robinson, E. L., Horne, K., Rae, F., & Abbott, T. M. C. 1993, *ApJ*, 411, 802
- Hatzidimitriou, D., Morgan, D. H., Cannon, R. D., & Croke, B. F. W. 2003, *MNRAS*, 341, 1290, astro-ph/0304297
- Hong, et al. 2005, in preparation
- Küpcü Yoldas, A. & Balman, S. 2002, *A&A*, 384, 190, astro-ph/0201111
- Laycock, et al. 2005, in preparation
- Martin, C. L., Kobulnicky, H. A., & Heckman, T. M. 2002, *ApJ*, 574, 663, astro-ph/0203513
- Moran, E. C., Filippenko, A. V., & Ryan, C. 2002, *ApJ*, 579, L71
- Porter, J. M. & Rivinius, T. 2003, *PASP*, 115, 1153
- Reid, I. N. & Hawley, S. L. 2000, *New Light on Dark Stars: Red Dwarfs, Low-mass Stars, Brown Dwarfs* (Berlin: Springer-Verlag)
- Rogel, A., et al. 2005, in preparation
- Silverman, J., et al. 2003, *Astron. Nachr.*, 324, 97

- Schlegel, D. J., Finkbeiner, D. P., & Davis, M. 1998, *ApJ*, 599, 525
- Smith, K.W., Lewis, G.F., Bonnell, I.A., Bunclark, P.S., & Emerson, J.P. 1999, *MNRAS*, 304, 367
- Steele, I. A., Negueruela, I., & Clark, J. S. 1999, *A&AS*, 137, 147, astro-ph/9906245
- The, P. S., Steenman, H. C., & Alcaïno, G. 1984, *A&A*, 132, 385
- Vanden Berk, D., et al. 2001 *AJ*, 122, 549
- Winkler, H., 1997, *MNRAS*, 287, 481
- Zhao, P., Grindlay, J., Edmonds, P., Hong, J., Jenkins, J., Schlegel, E., Cohn, H., & Lugger, P. 2003, *Astron. Nachr.*, 324, 176, astro-ph/0405509
- Zhao, P., et al. 2005, in preparation

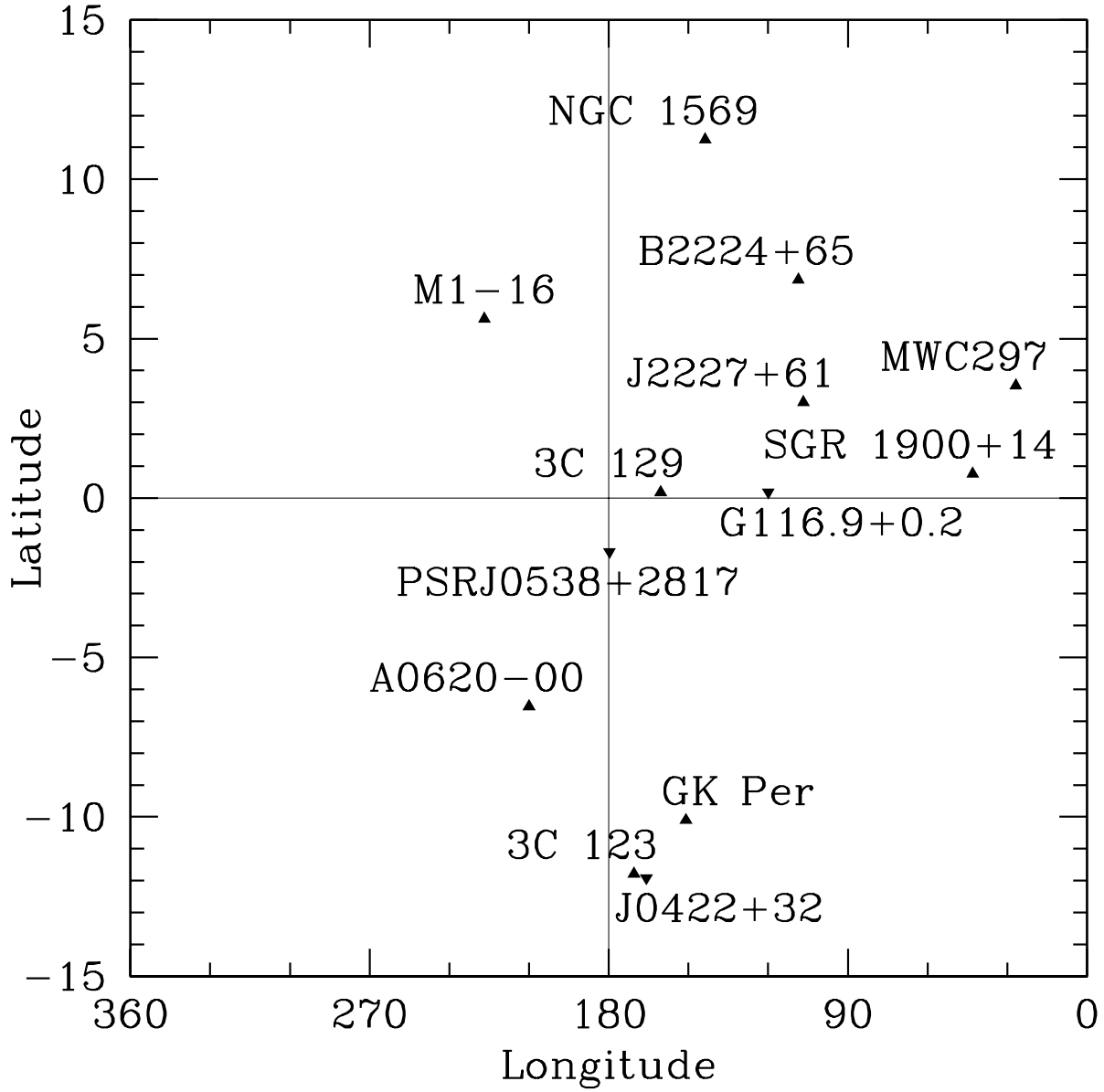


Fig. 1.— Field positions in Galactic coordinates. The actual field positions for J0422+32, PSRJ0538+32, and G116.9+0.2 are above the names, the rest are below the names.



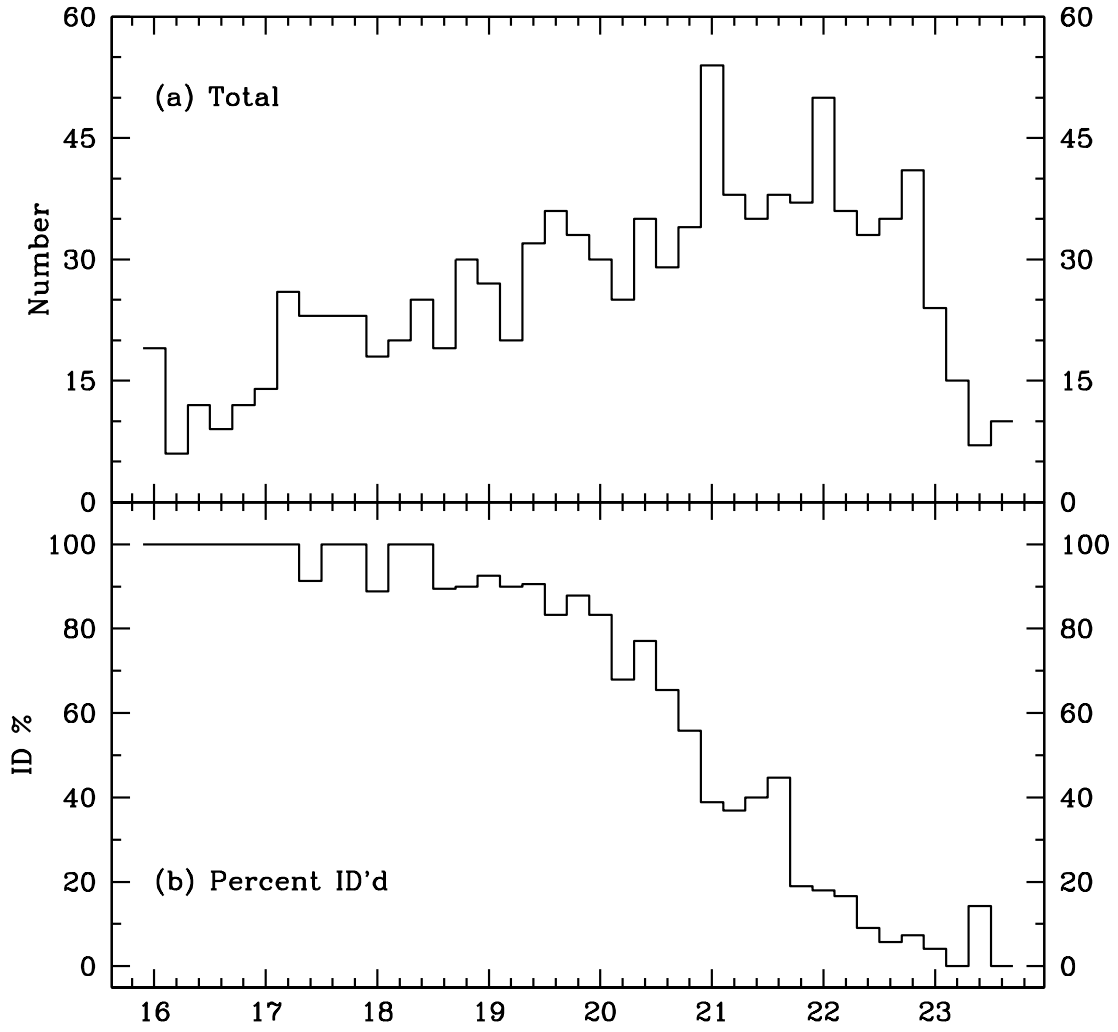


Fig. 2.— Histograms of R-band magnitude versus total observations (panel a) and classification rate (panel b).

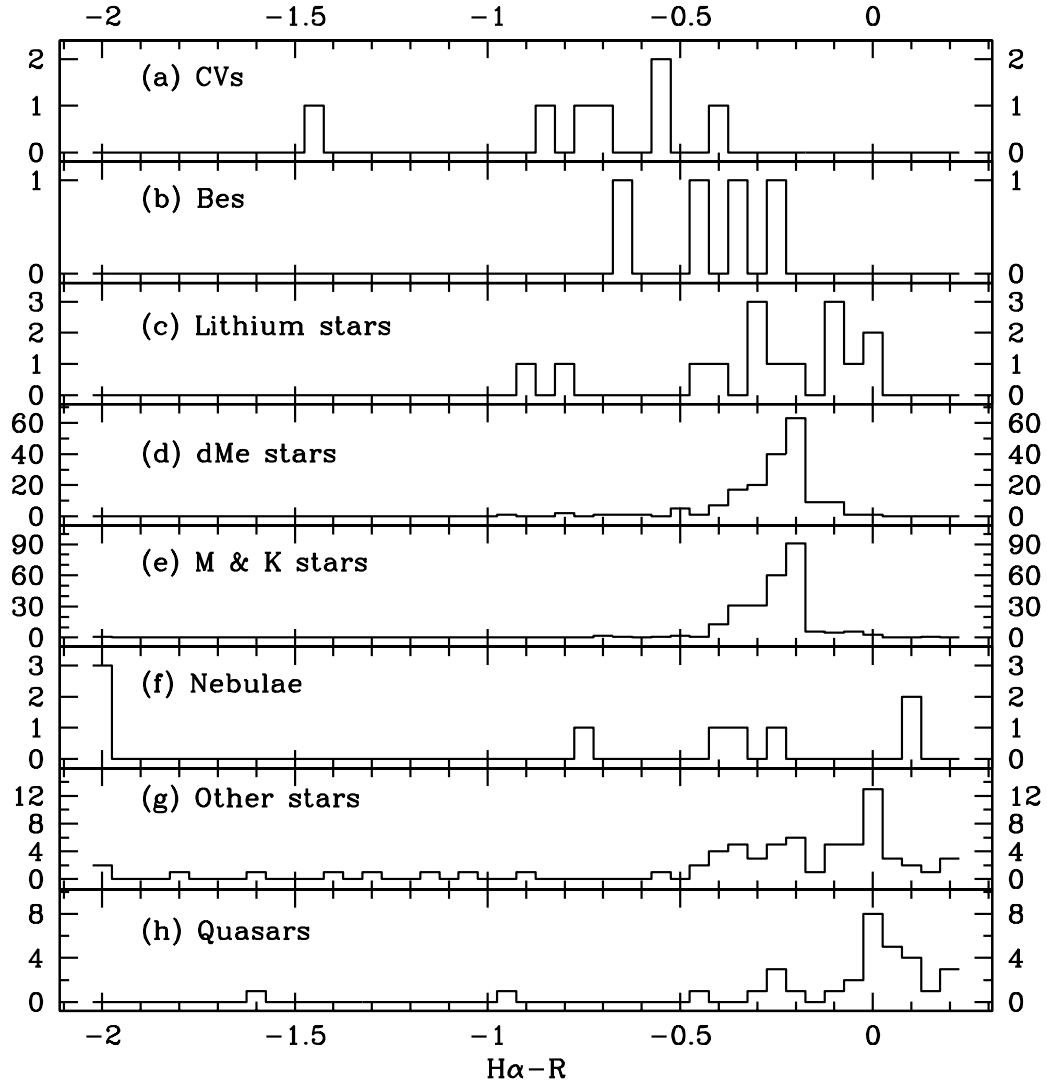


Fig. 3.— Histograms of  $H\alpha - R$  color of various object types detected in the project. The  $H\alpha - R$  color cutoff for non-X-ray objects of definite interest was at  $-0.3$ ; the cutoff for objects of marginal interest was at  $-0.2$ .

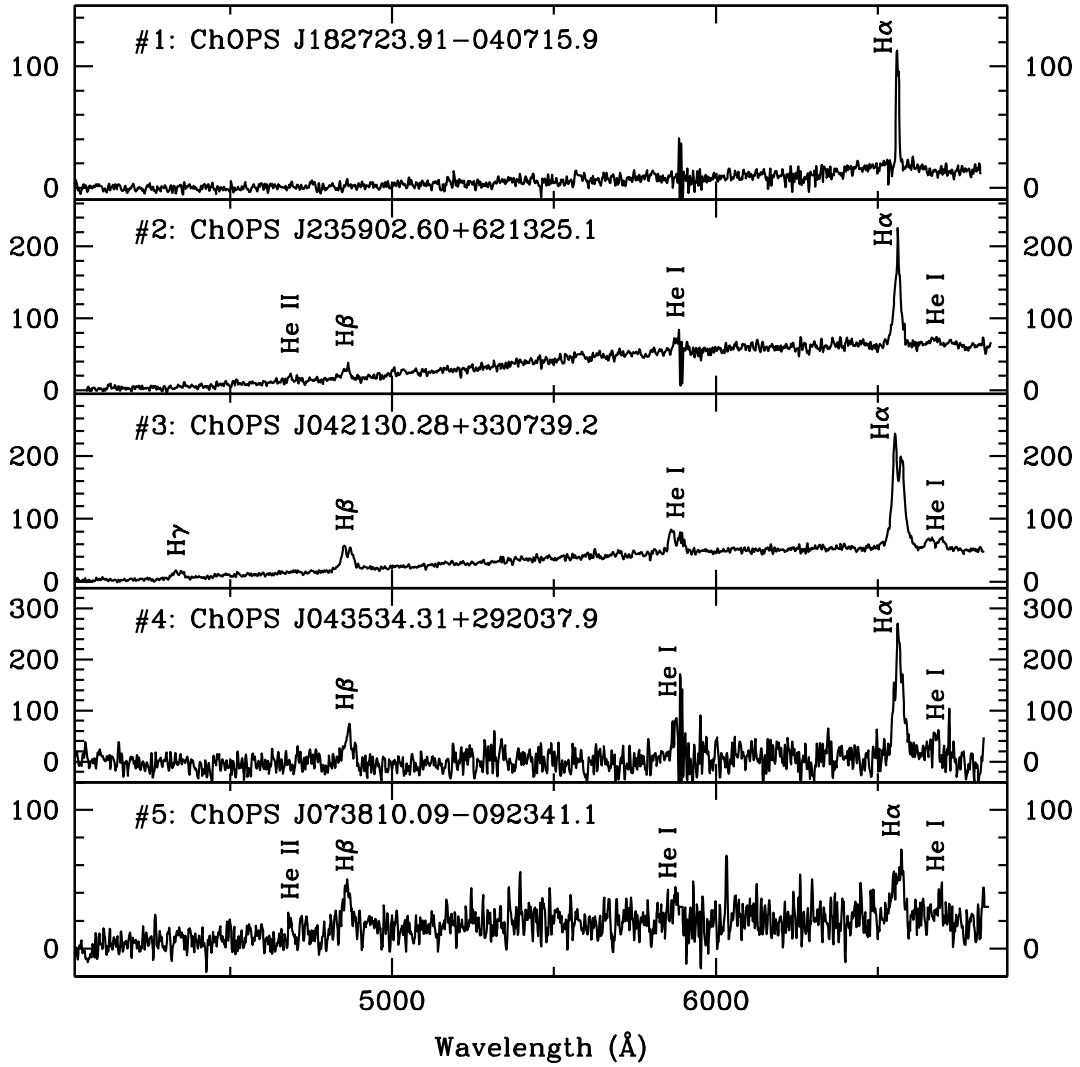


Fig. 4.— All new CV candidates detected to date, smoothed with a 3-channel boxcar filter.

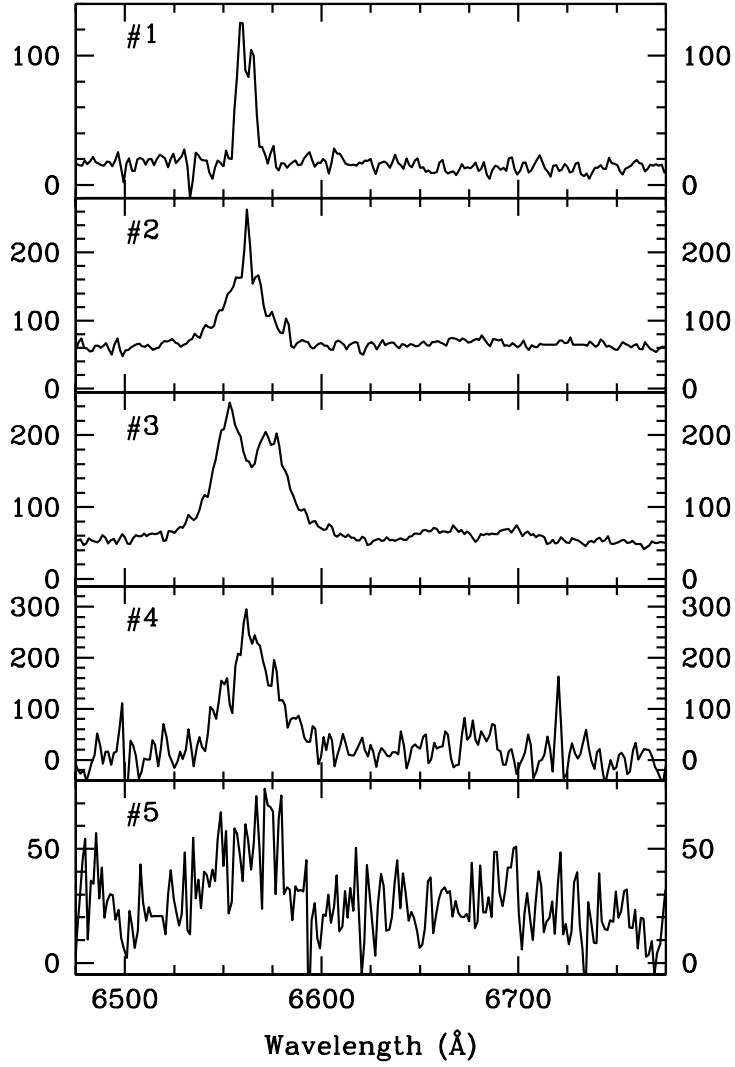


Fig. 5.— Unsmoothed H $\alpha$  and He I emission regions of all new CV candidate objects.

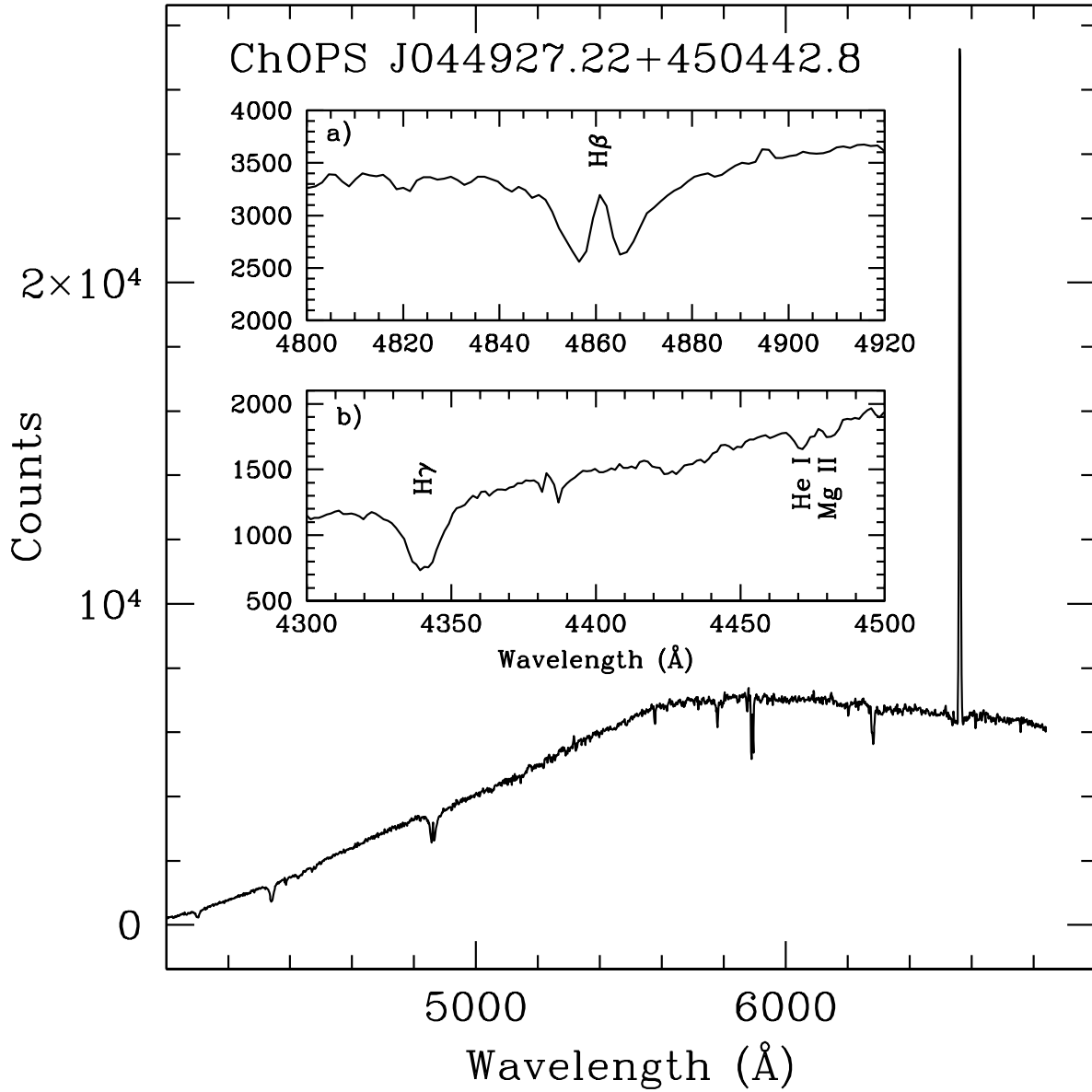


Fig. 6.— Candidate Be star ChOPS J044927.22+450443.8 in the 3C 129 field. Inset panel a) is the  $H\beta$  line, while b) is the  $H\gamma$  line and neighboring He I and Mg II lines ( $\lambda 4471$  Å and  $\lambda 4481$  Å).

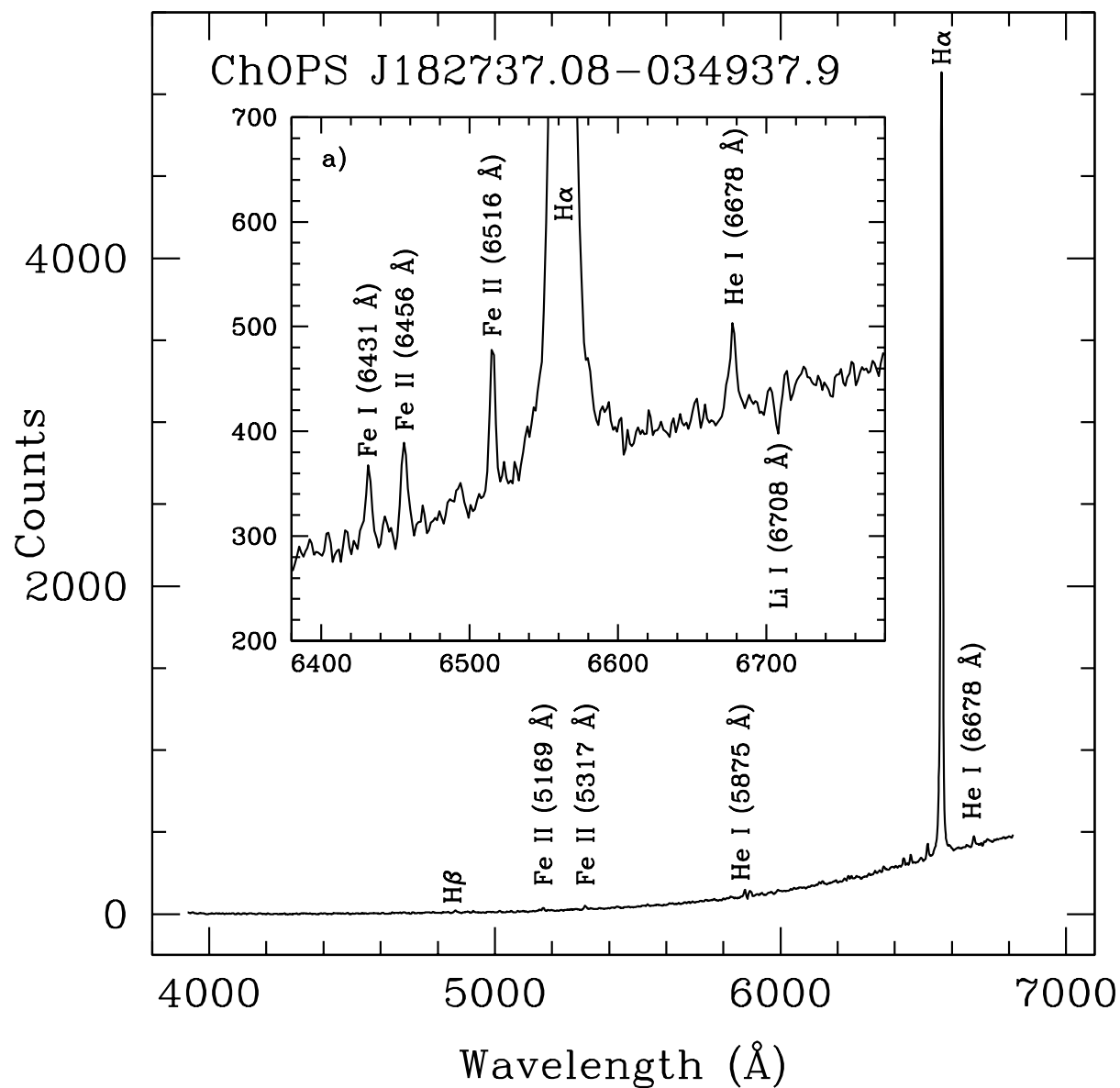


Fig. 7.— New T Tauri candidate object ChOPS J182737.08-034937.9. Inset panel a) shows the H $\alpha$  region of the spectrum, showing iron emission and lithium absorption lines as well as H $\alpha$  and He I emission.

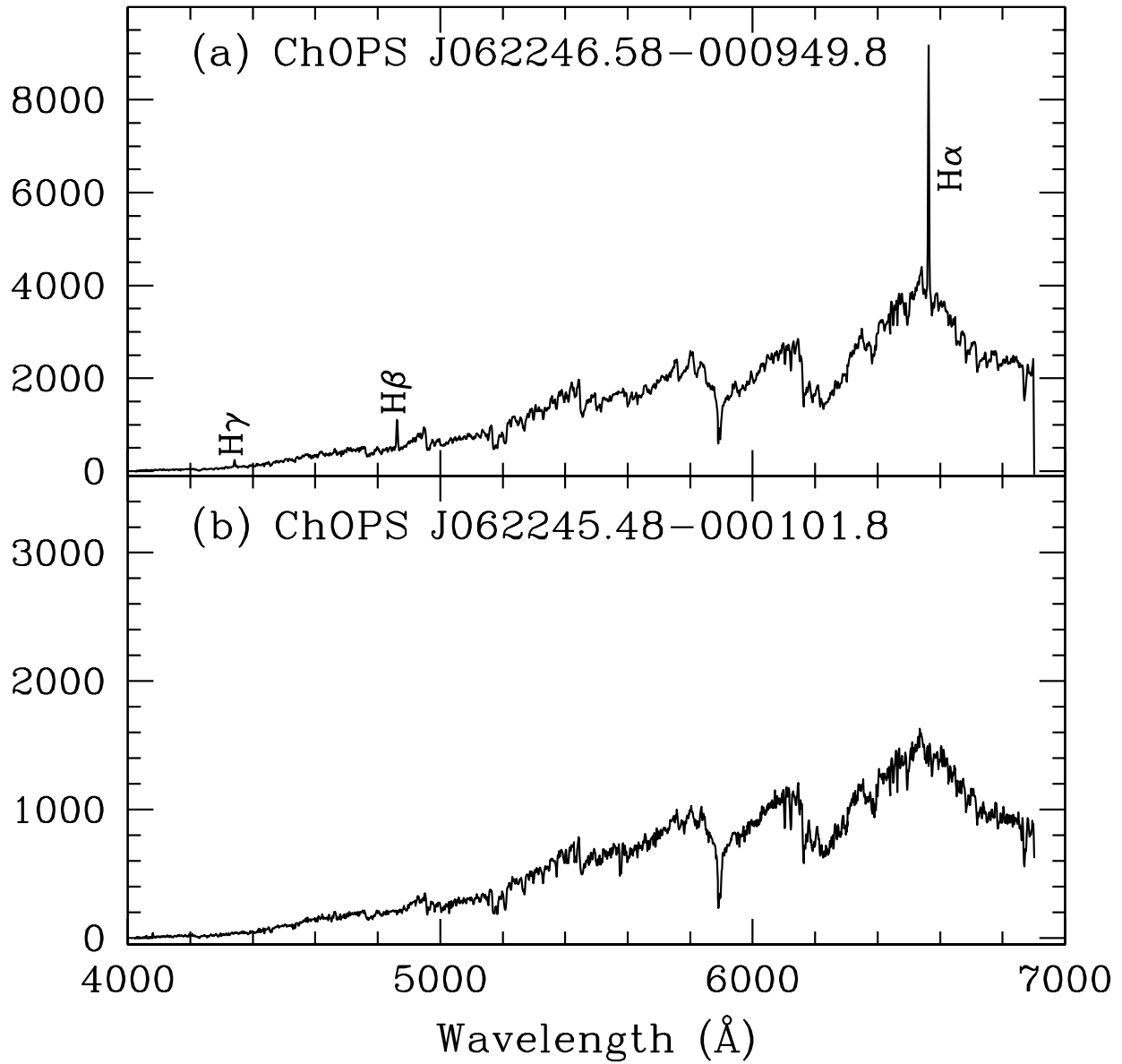


Fig. 8.— dM3e (panel a) and M3 star (panel b) spectra (from A0620 field).

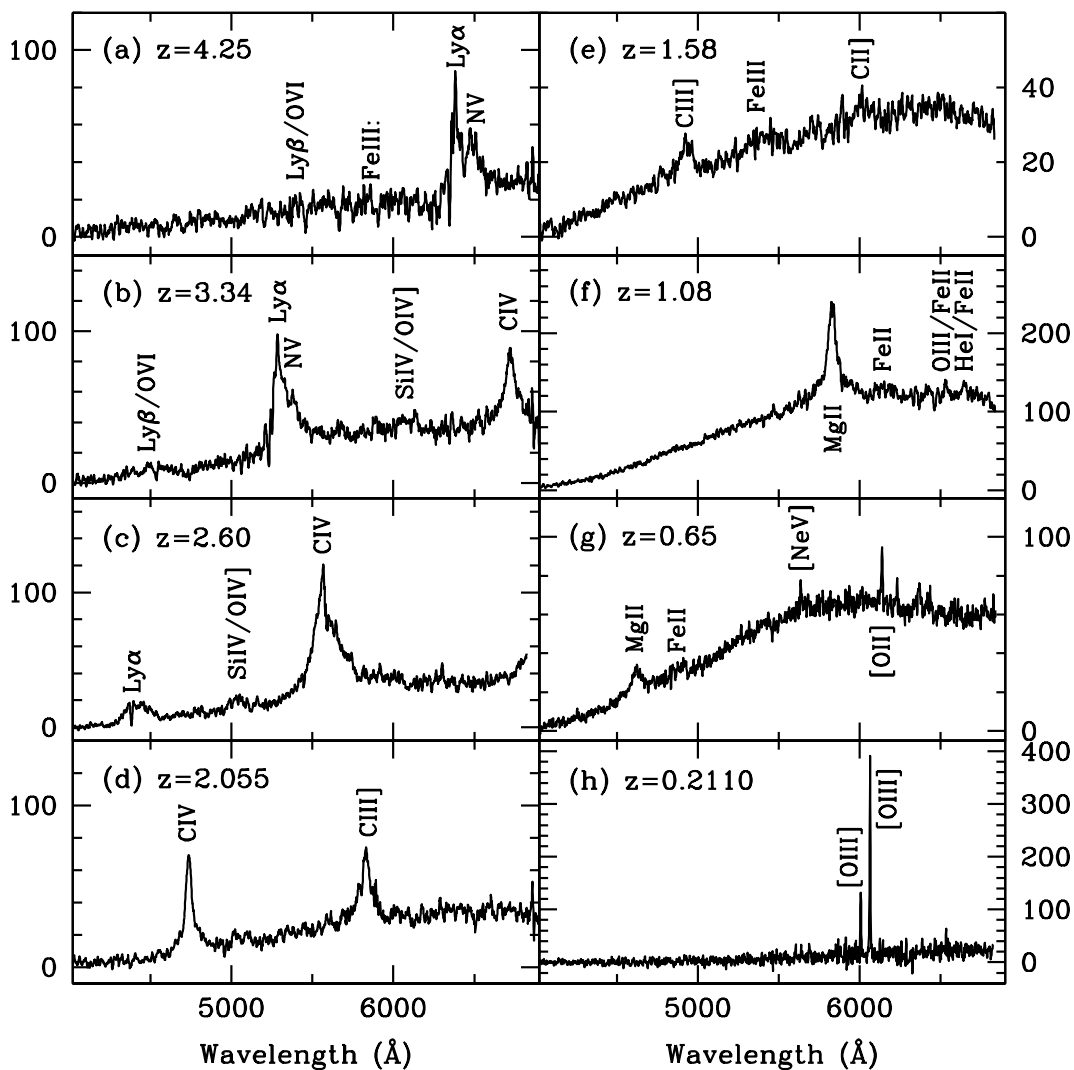


Fig. 9.— Representative quasar spectra from various fields in the ChaMPlane project. Most are regular broad-line objects, while (h) is a Seyfert II.



Table 1. Fields observed Jan 2001-Feb 2004.

Field	RA	DEC	l	b	$E(B - V)$
GK Persei	03:31.2	+43:54	151.0	-10.1	0.4
GRO J0422+32	04:21.7	+32:54	165.9	-11.9	0.3
NGC 1569	04:30.8	+64:50	143.7	11.2	0.7
3C 123	04:36.4	+29:38	170.5	-11.8	1.0
3C 129	04:49.3	+45:03	160.4	0.2	1.1
PSRJ0538+2817	05:38.0	+28:14	179.7	-1.7	1.4
A0620-00	06:23.3	-00:18	210.0	-6.5	0.5
M1-16	07:37.3	-09:39	226.8	5.6	0.2
MWC297	18:27.7	-03:50	26.8	3.5	20.4
SGR 1900+14	19:07.2	+09:19	43.0	0.8	4.2
B2224+65	22:25.9	+65:36	108.6	6.8	0.7
3EG J2227+6122	22:29.3	+61:19	106.7	3.0	1.7
G116.9+0.2	23:59.2	+62:24	116.9	0.2	0.8

Table 2. Summary of ChaMPlane-WIYN Observations.

Epoch	Field	Total Exp.(min.)
2001 Jan 23–25	J0422	300
...	A0620	300
2002 Jan 07–10	GK Per	420
...	J0422	280
...	NGC 1569	360
...	3C 123	420
2002 Aug 3-7	B2224	354
...	J2227	399
2002 Oct 2	3C 129	345
...	SGR 1900	180
2002 Oct 31	A0620	220
...	B2224	200
2002 Dec 5	A0620	235
...	B2224	200
2003 Jun 23–25	MWC297	440
...	SGR1900	360
...	J2227	170
2003 Sept 20–24	PSRJ0538	237
...	G116	340
2004 Feb 21–23	M1-16	60

Table 3. Observation summary by target type.

Target Type	Total Targets	Number Observed	Fraction Classified
X-ray	363	262	48%
H $\alpha$	1053	273	51%
H $\alpha$ M	1090	302	81%
Other	565	224	49%
Duplicate <sup>a</sup>	14	14	86%

<sup>a</sup>These objects appear both on the X-ray list and one of the H $\alpha$  lists.

Table 4. All CV and LMXB candidates observed to date.

Ref. #	Field	Name	RA	DEC	R mag.	XFOV <sup>a</sup>	notes
XB 1	A0620	A0620-00	06 22 44.56	−00 20 44.3	17.37	Y <sup>b</sup>	c
XB 2	J0422	J0422+32	04 21 42.71	32 54 27.1	20.83	Y <sup>b</sup>	d
CV 1	MWC297	ChOPS J182723.91-040715.9	18 27 23.92	−04 07 15.9	19.33	N	e
CV 2	G116	ChOPS J235902.60+621325.1	23 59 02.61	62 13 25.1	19.71	N	f
CV 3	J0422	ChOPS J042130.28+330729.2	04 21 30.28	33 07 29.2	20.33	N	...
CV 4	3C 123	ChOPS J043534.31+292037.9	04 35 34.32	29 20 37.9	21.65	N	...
CV 5	M1-16	ChOPS J073810.09-092341.1	07 38 10.10	−09 23 41.2	21.58	N	...

<sup>a</sup>Indicates whether the object is located in the *Chandra* ACIS field of view.

<sup>b</sup>This object was detected by *Chandra*.

<sup>c</sup>This object is known to be a LMXB with black hole primary (Haswell et al. 1993).

<sup>d</sup>This object is known to be a LMXB with black hole primary (Callanan, et al. 1996).

<sup>e</sup>This object has a definite M-star continuum present.

<sup>f</sup>This object has He II emission at  $\lambda 4686 \text{ \AA}$ .

Table 5. New Be star candidates.

Field	Name	RA	DEC	R mag.	XFOV <sup>a</sup>	Class
3C 129	ChOPS J044927.22+450443.8	04 49 27.22	45 04 43.8	13.61	Y	B5
J2227	ChOPS J223048.26+611453.7	22 30 48.26	61 14 52.7	15.13	N	late O
J2227	ChOPS J223030.43+612255.3	22 30 30.43	61 22 55.3	16.52	Y	early B
J2227	ChOPS J223013.39+613140.8	22 30 13.39	61 31 40.8	18.83	N	B

<sup>a</sup>Indicates whether the object is located in the *Chandra* ACIS field of view. None of these objects were detected by *Chandra*.

Table 6. Li stars.

Field	Name	RA	DEC	R mag.	XFOV <sup>a</sup>	EW <sup>b</sup>
MWC297	ChOPS J182737.07-034937.9	18 27 37.07	−03 49 38.0	17.13	Y	0.4
GKPer	CXOPS J033127.7+434623	03 31 27.60	43 46 22.4	16.51	Y <sup>c</sup>	0.4
NGC1569	CXOPS J043003.1+645142	04 30 03.18	64 51 42.6	17.88	Y <sup>c</sup>	0.4
J2227	CXOPS J222833.5+611105	22 28 33.51	61 11 05.7	15.09	Y <sup>c</sup>	0.3
J2227	ChOPS J222802.93+610430.1	22 28 02.94	61 04 30.2	16.86	N	0.5
SGR1900	CXOPS J190703.1+092215	19 07 03.23	09 22 14.5	17.14	Y <sup>c</sup>	0.3
B2224	ChOPS J222729.04+654026.2	22 27 29.04	65 40 26.3	17.86	N	0.4
B2224	CXOPS J222413.3+653628	22 24 13.67	65 36 26.4	17.04	Y <sup>c</sup>	0.4
B2224	ChOPS J222632.12+654954.7	22 26 32.12	65 49 54.8	16.18	N	0.6
A0620	ChOPS J062222.14-002515.2	06 22 22.15	−00 25 15.3	19.11	N	0.4
A0620	CXOPS J062159.6-001458	06 21 59.62	−00 14 56.2	...	Y <sup>c</sup>	0.2
MWC297	ChOPS J182649.73-035559.1	18 26 49.73	−03 55 59.2	17.71	N	0.6
J0538	ChOPS J053828.61+282845.8	05 38 28.61	28 28 45.9	18.76	Y	0.6
J0538	CXOPS J053831.5+281459	05 38 31.55	28 14 59.4	17.12	Y <sup>c</sup>	0.6
A0620	A0620-00	06 22 44.56	−00 20 44.3	17.37	Y <sup>c</sup>	0.2 <sup>e</sup>

<sup>a</sup>Indicates whether the object is located in the *Chandra* ACIS field of view.

<sup>b</sup>Equivalent width of the Lithium  $\lambda 6708\text{\AA}$  absorption line.

<sup>c</sup>This object was detected by *Chandra*.

<sup>d</sup>This target was off the Mosaic field of view.

<sup>e</sup>A0620-00 is known to have high lithium abundance(González Hernández, et al. 2004).

Table 7. Quasar candidates detected to date by ChaMPlane/WIYN.

Field	Name	RA <sup>a</sup>	DEC <sup>a</sup>	R mag.	z	Conf. <sup>b</sup>	Notes
NGC1569	CXOPS J043041.4+643925	04 30 41.21	64 39 25.6	21.24	0.2110	5	c,d
NGC1569	CXOPS J043125.1+645154	04 31 25.13	64 51 54.3	20.04	0.279	5	c,e
J0422	ChOPS J042048.59+324521.9	04 20 48.59	32 45 22.0	22.71	0.3070	5	c,f
J0422	ChOPS J042051.71+324533.8	04 20 51.72	32 45 33.8	23.50	0.3099	5	c,f
J0422	CXOPS J042211.8+325605	04 22 11.83	32 56 04.3	20.39	0.65	4	...
GKPer	CXOPS J033105.9+440328	03 31 05.95	44 03 27.6	20.41	0.93	5	...
GKPer	CXOPS J033136.5+434209	03 31 36.66	43 42 11.3	19.96	1.08	5	h
J0422	CXOPS J042155.0+330037	04 21 55.04	33 00 36.3	21.03	1.125	4	...
B2224	CXOPS J222456.1+653131	22 24 56.21	65 31 31.5	22.27	1.13	2	...
G116	CXOPS J235813.4+622447	23 58 13.47	62 24 47.8	21.57	1.29	4	...
3C123	CXOPS J043657.6+294155	04 36 57.63	29 41 55.5	21.28	1.30	3	...
J0422	CXOPS J042127.7+325038	04 21 27.76	32 50 38.3	22.07	1.31	3	...
J0422	ChOPS J042140.57+331204.1	04 21 40.58	33 12 04.1	21.15	1.35	2	f
J0422	ChOPS J042028.32+325239.7	04 20 28.32	32 52 39.8	22.44	1.40	3	g
J0422	CXOPS J042201.0+325237	04 22 00.97	32 52 36.4	20.92	1.58	3	...
J0422	CXOPS J042155.1+324726	04 21 55.08	32 47 26.0	20.98	1.845	5	...
GKPer	CXOPS J033112.2+433844	03 31 12.16	43 38 44.4	20.70	1.85	4	...
J0422	CXOPS J042117.5+330206	04 21 17.46	33 02 05.5	19.23	1.93	3	...
J0422	CXOPS J042140.7+324941	04 21 40.83	32 49 40.7	22.82	1.94	4	...
G116	CXOPS J235813.2+623343	23 58 13.29	62 33 44.6	21.11	2.04	5	...
J0422	CXOPS J042133.8+325557	04 21 33.84	32 55 57.7	21.07	2.055	5	...
A0620	CXOPS J062240.4-002113	06 22 40.47	-00 21 13.6	22.65	2.20	5	...
J0422	CXOPS J042201.6+325730	04 22 01.58	32 57 29.3	21.56	2.203	3	...
GKPer	CXOPS J033120.7+434002	03 31 20.64	43 40 01.2	21.56	2.60 ± 0.03	4	...
J0422	CXOPS J042154.3+325310	04 21 54.39	32 53 09.8	21.55	2.91	5	...
B2224	CXOPS J222525.0+652917	22 25 25.17	65 29 17.7	22.31	3.06	3	...
M1-16	CXOPS J073749.6-094432	07 37 49.73	-09 44 31.7	23.05	3.18	3	...
J0422	CXOPS J042210.3+330126	04 22 10.35	33 01 26.0	21.12	3.34	5	...
J0422	ChOPS J042200.24+325708.0	04 22 00.25	32 57 08.0	22.01	4.25	3	g

<sup>a</sup>RA and DEC are taken from the optical counterpart positions.

<sup>b</sup>Confidence of redshift determination (based on line identifications): 5=highest, 2=low. Possible quasars with confidence of 1 were not included in the table.

<sup>c</sup>This object appears to be a narrow-line AGN.

<sup>d</sup>This object is likely a Seyfert II, by comparison with spectra in Moran, Filippenko, & Ryan (2002).

<sup>e</sup>This object is in the literature (Martin, Kobulnicky, & Heckman 2002) as CXOU J043125.1+645154 as an AGN.

<sup>f</sup>This object was not in the *Chandra* field of view.

<sup>g</sup>This object was in the *Chandra* field of view but was not detected.

<sup>h</sup>This object is in the literature (Küpcü Yoldas & Balman 2002) as 1RXH J033136.5+434213 as an X-ray source.